

We thank the reviewer for his constructive comments. Responses to the comments and suggestions made in Paragraph 3 of the review are provided below, along with the proposed amendments (italicised).

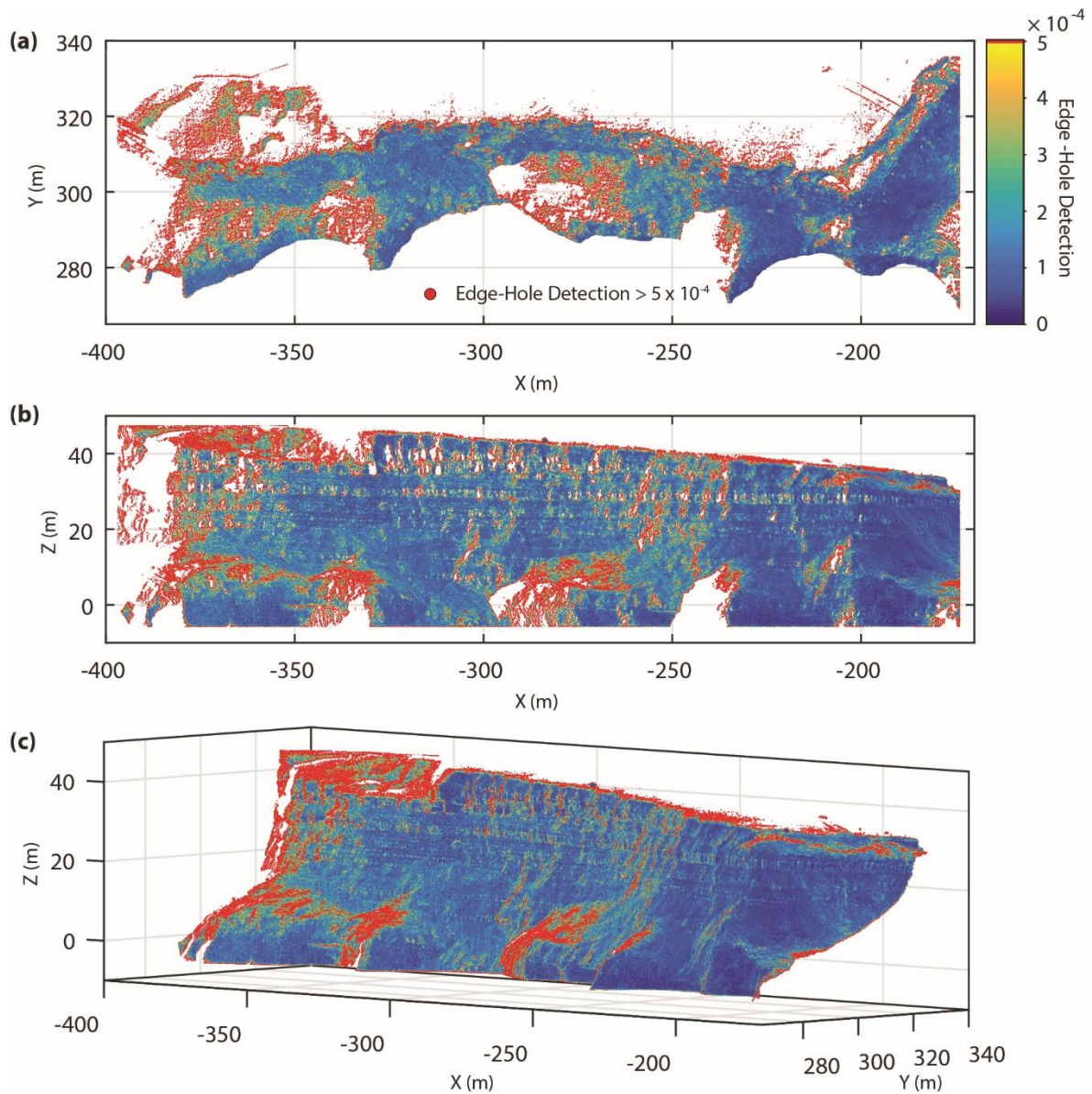
“In my view the main limitation of the method proposed here is to pass by a raster to estimate volumes. However this point is properly discussed, and an error on the volume estimation is proposed”.

We agree that this presents a limitation and have highlighted the potential for 3D volume estimation, with reference to recently published work on this topic. As discussed in the text, rasterising was undertaken due to the structure (primarily occlusion) and high frequency of data, which necessitated an efficient processing algorithm.

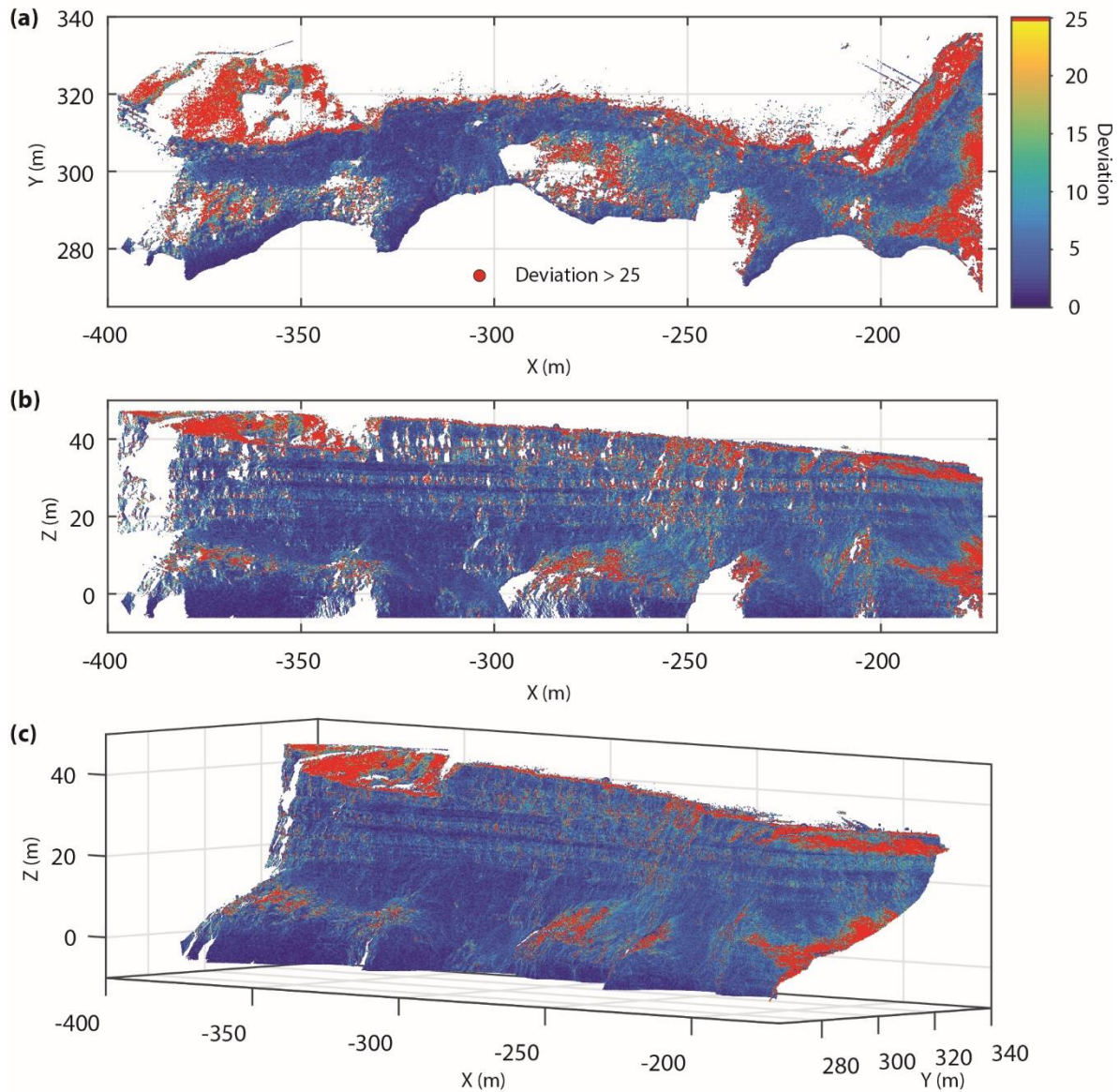
“I had to read several times the text of page 5 and the caption of Fig 3 before to understand the meaning of this figure. It would be useful to develop a bit more this part. I find it confusing in the present form.”

The reviewer highlights some confusion regarding Fig. 3 (the selection of a threshold edge-hole value) based on its description in text and in the figure caption, specifically around the function of this step in our processing. In light of this, in text amendments are provided below. Additionally, we feel that examples of East Cliff coloured by the EH value would be ideally suited to a supplementary information, alongside the same figure coloured by the deviation filter. Both figures are also provided below.

Text to add - P13 L20: In order to select a threshold EH value, the epistemic error between two point clouds was quantified once EH values above a specific threshold were removed. As the threshold is increased, fewer points are filtered from each cloud. The theoretical distance between the two point clouds is assumed to be zero given that no rockfall were observed between their collection. Any offset therefore represents the epistemic uncertainty, which is quantified for this purpose as the standard deviation of a 3D change detection. This uncertainty is plotted against the applied threshold in Fig. 3a. As the threshold is increased, points with higher EH values are retained and the offset between the two point clouds also increases. The distribution of EH values across the cloud is presented in Fig. 3b. Using a 1 m search radius, an inflection at the 95th percentile of points occurs at 5×10^{-4} . As a threshold, this value typically removes 5% of points, which, as depicted by the dashed line in Fig. 3a, account for uncertainties > 0.5 m. In addition to identifying edge features on the cliff face, this also helps to delineate areas of occlusion within the point cloud. The point density in Eq. 1, k , is used to filter spurious ‘floating points’ in the dataset (for example birds or dust). k values < 4 , the minimum number to accurately define a centroid with an associated error, were removed.



Supplementary information, Figure 1: Edge-Hole values across the cliff with values $> 5 \times 10^{-4}$ coloured red and removed from each point cloud prior to change detection. Edge-Hole values above the applied threshold occur predominantly around occluded areas but also along protruding sandstone at the cliff top. Areas of the cliff face that appear blue (i.e. low EH values) correspond with bedding that is draped with silt from the interbedded siltstones and carbonaceous mudstones above. (a) Aerial perspective. (b) x-z plane directly viewing the cliff. Holes in the point cloud are now apparent, with their edges delineated in red. (c) View from the scanner position.



Supplementary information, Figure 2: Deviation across the cliff with values > 25 coloured red and removed from each point cloud prior to change detection. (a) Aerial perspective showing high deviation returns at the cliff top and on top of the buttress, which has both steeper incidence angles, high surface roughness from fallen boulders and in some areas vegetation growth. (b) x-z plane directly viewing the cliff. (c) View from scanner position.

“Fig 7: I did not get the complete message of this caption. Maybe you can split the different elements in several sub-figures (pre vs post, sign ambiguity, sensitivity)”

The reviewer notes that the purpose of Fig. 7 is unclear in its present form. As suggested, we have amended the figure and its caption, as below. The amended figure no longer contains the dashed lines representing vector sign ambiguity, given that this information is unnecessary in the context of point cloud selection for normal estimation. The figure is now also split in two for greater clarity. As highlighted in the figure caption, both (a) and (b) are point vectors estimated from the same position on the rock face, the only difference is their estimation pre- or post-rockfall.

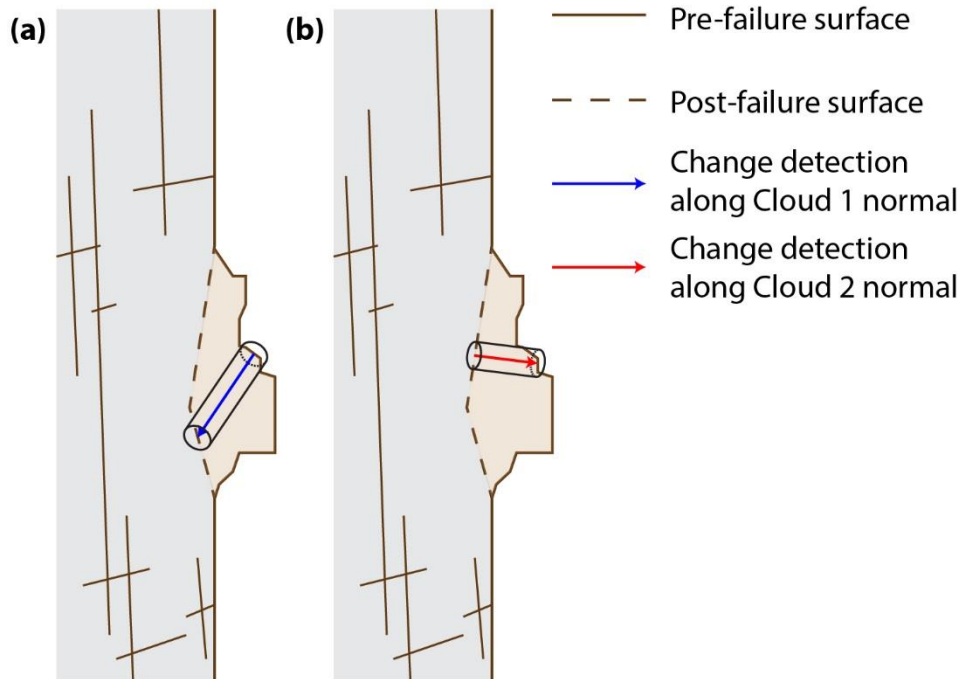


Figure 7: Conceptual variation in the distance along the normal for a rockfall. (a) Change detection along a surface normal direction estimated from the pre-failure surface (Cloud 1). (b) The normal direction estimated using a planar, post-failure surface more accurately represents the direction of change than the post-failure surface vector, due to the complexity of the pre-failure surface. With both change detections originating in the same approximate positions on the cliff face, the difference in vector lengths illustrates the sensitivity of the 3D change measurements to the normal estimation.

“Acronym DAN not defined (dist along normal)”

We have amended the relevant sentence to the following:

P12 L 18: *To address this, a distance along the normal with variable cylinder length (DAN VCL) for each point is used.*

“M3C2: it would help to have an extra figure here to explain the geometry of the cylinder and its relations with the point clouds”

The reviewer suggests that a figure would be useful to explain the geometry of the cylinder with respect to the point cloud. While Figure 3 from Lague et al. (2013:7) underpins and clearly describes the M3C2 approach, we have opted to use a subset of points from within the area of a rockfall on the rockface. A new figure is presented below, which is intended for inclusion within the main text (approximate location P11 L4). This depicts many of the terms described in Section 3.4. Subsequent figures and cross references have been amended to reflect the inclusion of this eighth figure.

P10 L23: *The distance calculation used is based upon the structure of the M3C2 algorithm, developed by Lague et al. (2013). We describe below a modification incorporated to improve the overall accuracy of change detection and to streamline the workflow when applied to large time series scan datasets. Once the normal vector is*

estimated, a bounding cylinder with a user-defined radius is created along the normal running through the query point. In order to enforce the boundaries of this cylinder, the orthogonal distance between every point within the current and neighbouring 26 octree cubes and the normal vector was estimated:

$$\hat{d} = [X_n, Y_n, Z_n] - [X_p, Y_p, Z_p] \quad (8)$$

where \hat{d} is a vector that connects each neighbour point p to a point on the normal vector \hat{n} , such as the query point, q . The projection of each point onto the normal P is therefore:

$$P = q \times \hat{d}, \text{ or} \quad (9a)$$

$$P = q + \left(\frac{\hat{d} \cdot \hat{n}}{\hat{n} \cdot \hat{n}} \right) \times \hat{n} \quad (9b)$$

and the orthogonal distance is:

$$d_{\text{orth}} = \sqrt{(X_n - X_p)^2 + (Y_n - Y_p)^2 + (Z_n - Z_p)^2} \quad (10)$$

Given that the position of each neighbouring point and its orthogonal distance to the normal vector are known, the cylinder boundaries can be enforced using the user-defined cylinder radius, r , retaining only points where $d_{\text{orth}} \leq r$ (Fig. 8). Once the points, c , in the cylinder are isolated for both point clouds, the mean point CoG is estimated by:

$$\text{CoG} = \left(\frac{\sum_{i=1}^{k_c} x}{k_c}, \frac{\sum_{i=1}^{k_c} y}{k_c}, \frac{\sum_{i=1}^{k_c} z}{k_c} \right) \quad (11)$$

where k_c is the number of points in c . Both mean points are then projected onto the normal vector using Eq. 9a and Eq. 9b. The mean projected points of each sub-cloud, CP , are subtracted to give a distance vector, \hat{v} :

$$\hat{v} = CP_2 - CP_1 \quad (12)$$

If the vector of change is along the direction of the normal vector (forward movement), the dot product of both vectors is > 0 . If the vector of change is counter to the normal direction (backward movement), the dot product is < 0 and the vector is inverted.

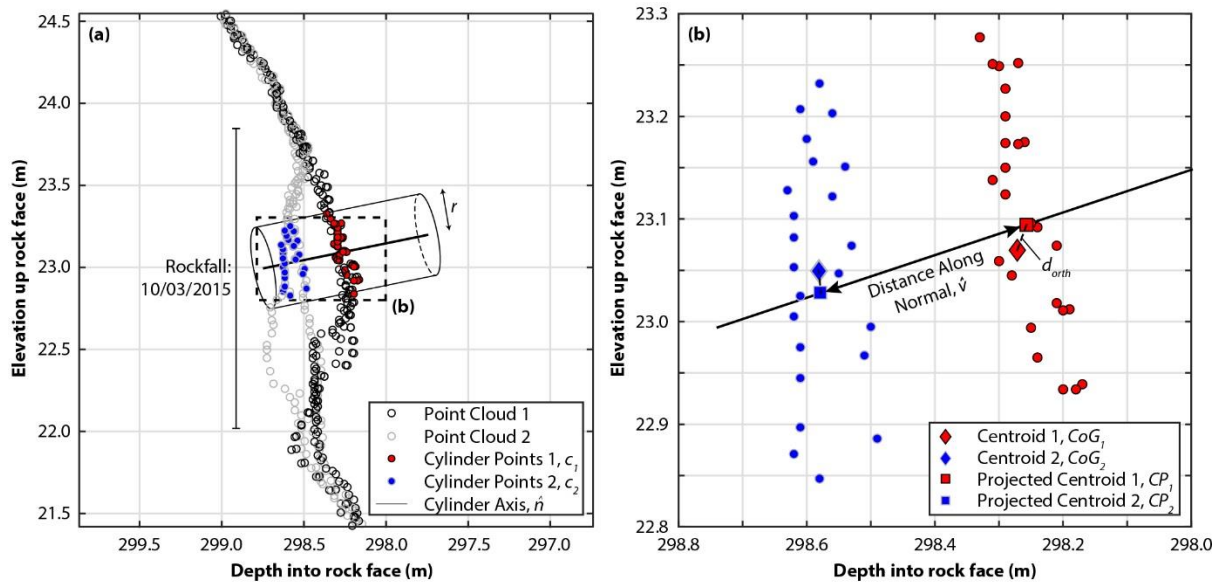


Figure 8: (a) A 2 m wide transect taken mid-way up East Cliff. The black points are taken from Cloud 1 and the grey from Cloud 2, with a 1.75 m high rockfall clearly shown. Points within the cylinder radius, which intersects the two clouds, are shown as red and blue. The cylinder axis, which travels through the query point, is also shown, (b) Area of intersect selected from (a) the centroids of each point cloud are determined and their orthogonal projection onto the normal vector (cylinder axis) is estimated (dashed lines). The distance measured in this study is between these projections, along the normal

“Acronyms LoD and CoG are not defined at their first occurrence.”

The reviewer notes that neither LoD nor CoG are defined in the first instance. In light of this, the following alterations have been made:

P6 L28: ... thereby lowering the Level of Detection (LoD) that could be applied ...

P5 L5: ... central position of the neighbourhood points (CoG) calculated ...

“N is the number of cells that delimit the event”; isn’t it a bit ambiguous to use the verb ‘delimit’ to define N, with regards to Nb?”

The reviewer notes that the use of the word ‘delimit’ is unclear with respect to the number of cells that comprise a rockfall. We recognise this and propose the following amendment:

P14 L1: where N is the number of contiguous cells that are classified as volume lost ...

“Complete Eq 16 and 18c with the results of the calculations”

The reviewer suggests completing Eq 16 (the maximum area uncertainty of a set of volume loss pixels) and Eq 18c (the estimation of area uncertainty used here). Both Eq 16 and Eq 18c underpin our volumetric uncertainty

estimation (Eq. 19) .The results of Eq 18c are therefore presented in Fig. 10b for the entire rockfall dataset, and discussed on P16 L4 as the volumetric uncertainty.

“I would ‘remove the areas BELOW the error threshold”

The reviewer highlights a mistake in our wording regarding the removal of failures whose area is *below* the maximum area error.

P14 L14: *This value can be applied as a threshold to the rockfall inventory, such that failure areas below $A_{maxerror}$ are removed.*

“The term ‘risk’ is not appropriate here as it includes many other things than the block release frequency. Suppress this sentence.”

Given the absence of other factors that constitute risk estimation, the reviewer highlights that the term risk is inappropriate in the context of the frequencies observed here.

P18 L 30: *[Sentence removed as suggested].*

References used in this response

Lague, D., Brodu, N. and Leroux, J.: Accurate 3D comparison of complex topography with terrestrial laser scanner: Application to the Rangitikei canyon (NZ), ISPRS J. Photogramm., 82, 10-26, 2013.